Numerical Study of Jet Inverse Diffusion Flames Issuing from an Elliptical Burner

Ahmed A. Mahgoub
Continuous Combustion Laboratory, Mechanical Power Engineering Department, Faculty of Engineering at El-Mataria, Helwan University

Mohamed S. Mohamed Gamal
Continuous Combustion Laboratory, Mechanical Power Engineering Department, Faculty of Engineering at El-Mataria, Helwan University

Ahmed M. Abdulnaim

https://doi.org/10.5109/7158030

出版情報：Proceedings of International Exchange and Innovation Conference on Engineering & Sciences (IEICES). 9, pp.397-404, 2023-10-19. 九州大学大学院総合理工学府
バージョン：

Numerical Study of Jet Inverse Diffusion Flames Issuing from an Elliptical Burner

Ahmed A. Mahgoub[1,*], Mohamed S. Mohamed Gamal[1], Ahmed M. Abdulnaim[1]
[1]Continuous Combustion Laboratory, Mechanical Power Engineering Department, Faculty of Engineering at El-Mataria, Helwan University, Cairo 11718, Egypt
*Corresponding author email: ahmed_mahgoub93@m-eng.helwan.edu.eg

Abstract: *The present study numerically examines the influence of the central air velocity on the combustion characteristics of Inverse Diffusion Flames (IDFs) of an elliptical burner under a constant thermal input. The burner configuration consists of a central circular air pipe surrounded by an annular elliptical fuel tube. The computational model is benchmarked with a previous experimental work that utilized Liquefied Petroleum Gas (LPG) as the fuel. The simulations were conducted using various turbulence models, as well as detailed and simplified LPG compositions. The flame structure is affected by the elliptical shape of the fuel jet, which generates different radial profiles on both major and minor axes. The results indicate that the simplified LPG can achieve comparable results with lower computational expense. Moreover, augmenting the air velocity lowers the flame temperature and consequently reduces NO_X concentrations. CO concentration also diminishes with increasing the air velocity due to the improved mixing and entrainment.*

Keywords: Inverse Diffusion Flame (IDF); Elliptical Burner; CFD

1. INTRODUCTION

Combustion is a multifaceted process that involves chemical reactions, heat and mass transfer, fluid dynamics, and turbulence. It has widespread applications in power generation, propulsion, heating, and industrial processes. However, combustion also presents several challenges, including pollutant emissions, flame stability, and combustion efficiency [1]. Therefore, gaining a comprehensive understanding of the combustion process and optimizing its performance is crucial for mitigating environmental impact.

Flame configuration is a crucial aspect of combustion that determines the mixing and reaction characteristics of fuel and oxidizer streams. Depending on the relative position of fuel and oxidizer jets, flames can be classified into normal diffusion flames (NDF), inverse diffusion flames (IDF) [2]. Diffusion flame, as arguably the most prevalent types of flame in systems of combustion, with a central fuel jet surrounded by an outer oxidizer jet. IDFs are a special type of non-premixed flame, that changes from the normal diffusion flame in regard to air and fuel jets position. The IDF, an external fuel jet surrounds the central air jet, which is then entrained inward by the high-velocity air jet to combine with the air to create a partially premixed flame. If not, it might primarily burn in the diffusion mode.

The flammability limit of the typical diffusion flame is quite broad. While the premixed flame exhibits low soot formation characteristics. IDF reveals the features associated with premixed and diffusion flames, thus, can take the merits of both of flames such as lower emissions of soot and NOx, wider flame stability, and higher operational safety [3, 4]. The IDF is more hygienic than NDF and is less susceptible to the phenomena of the lift off and flash back when contrasted to a premixed flame. As a result, it is interesting to see whether using IDFs in residential and commercial applications for heating is feasible. IDFs also exhibit unique flame structures and dynamics that differ from NDFs [5]. For example, IDFs can have multiple flame branches depending on flow conditions and burner geometry. They can also undergo flame extinction and re-ignition phenomena due to local quenching or global blowout. Additionally, IDFs can be influenced by various factors, such as co-flow, fuel composition, and burner configuration [4].

Several previous investigations have been conducted to better understand the characteristics of IDFs. The length of the laminar IDF increases in proportion to the air flow rate. [6, 7]. The nozzle diameter and air and fuel flow rates also have an influence on IDF height, the structure and heating characteristics,. [8]. The centerline temperature distribution and flame appearance are both influenced by the air-fuel ratio [9]. The impact of different air/fuel velocity ratios at a constant flow rate of fuel on the flame structure was examined to achieve the merging and entrainment roles in IDF [5, 10]. The influence of burner arrangement effects the IDFs thermal structure owing of the merging excellence among air and fuel [4]. Moreover, IDF heat transfer characteristics are influenced by the airport's diameter [11]. Additionally, the flame shape, centerline temperature, and CO concentrations are provided along with the Reynolds number impacts and equivalence ratios [12]. The swirl stabilized IDF's characteristics, such as flame appearance, heat transfer, and emissions, are described in [1, 2, 13]. Another researches inspected the IDF characteristics experimentally as well as computationally, they examined the flame appearance, the flame length, and centerline temperature distribution [14, 15].

Elliptical jets have received less attention in the literature than circular jets for IDFs. Elliptical jets offer the advantage of greater flexibility in controlling jet spreading and entrainment by varying the aspect ratio of the ellipse. They can also produce different flow patterns and mixing behaviors than circular jets due to the presence of vortex pairs along the major axis of the ellipse. Therefore, studying the combustion characteristics of IDFs with elliptical jets can provide new insights into the impacts of jet shape on the structure of the flame and dynamics.

The limited availability and negative effects of fossil fuels on the environment have increased the need for

using sustainable fuels in different energy and thermal processes. Methane and liquefied petroleum gas (LPG) are two of the possible alternatives that are widely accessible and adaptable, but they also have their pros and cons. Methane burns cleanly and lowers greenhouse gas emissions, but it is difficult to store, transport and prevent leakage [16, 17]. LPG is a cheap and plentiful fuel that can enhance the performance of combustion engines and lower NO_X emissions, but it also has a lot of carbon and needs special care and precautions [18, 19]. Therefore, it is important to compare these fuel options and follow best practices to maximize their benefits and reduce their harms to the environment and society.

This paper presents a numerical study of jet inverse diffusion flames (IDFs) issued from an elliptical burner. It provides new insights into the effects of fuel jet shape on the flame structure. The objective of this study is to investigate the impact of air velocity on the flame and combustion characteristics of IDFs with elliptical jets at constant thermal input. The computational model is validated with previous experimental work using liquefied petroleum gas (LPG) as the fuel and air as the oxidizer. Different computational models are investigated to achieve the most appropriate one for the current burner. The study contributes to the understanding of IDFs with elliptical jets and their potential applications in energy and thermal processes.

2. METHODOLOGY

The current study aims to construct a computational model that can simulate the inverse diffusion flame (IDF) emanating from an elliptical burner and elucidate the complex physical and chemical processes involved in such flames. The model is validated by comparing it with previous experimental data on an elliptical burner [20]. The steady-state RANS simulations were performed using ANSYS CFX 19 software. The following sections describe the preparation and setup of the simulation, as well as the models and their respective governing equations.

2.1 Burner Geometry

This study investigates a vertical elliptical IDF burner that has three concentric streams: an inner circular air stream, an elliptical fuel stream, and an outer secondary elliptical air stream. Fig. 1 illustrates the burner configuration. The inner circular air stream has an outer diameter of 8 mm, and the fuel elliptical tube has a major axis of 30 mm and a minor axis of 15 mm, resulting in an aspect ratio of 2:1. The outer elliptic tube has the same aspect ratio, with a major axis of 70 mm and a minor axis of 35 mm. The outer secondary air stream is not considered in the present study. The burner geometry is simplified by modeling only a quarter of the domain, using two symmetry planes: the major and minor planes of the fuel elliptic tube. Fig. 2 shows the model domain and the symmetry planes. Fig. 2 and Fig. 3 demonstrate the geometry dimensions.

The model focuses on the flame zone outside the burner and neglects the upstream flowfield from the burner exit. This simplification is justified by the fact that the burner has a straightforward geometry without any complex interior features. To ease the grid generation process, the bottom face of the model, which corresponds to the exit plane of the burner, was divided into several geometries as depicted in Fig. 3.

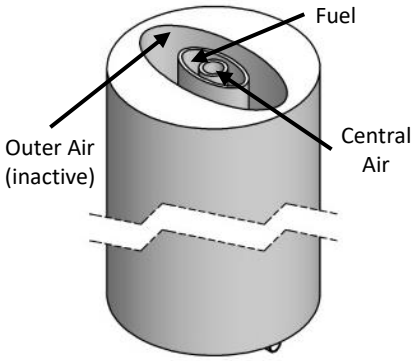

Fig. 1. The elliptical IDF burner configuration [20].

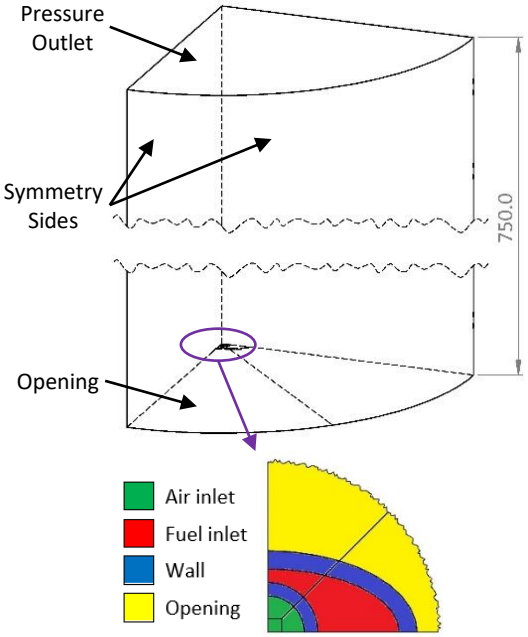

Fig. 2. A 3-D view of the quarter computational domain of the elliptical burner superimposed with the boundary conditions.

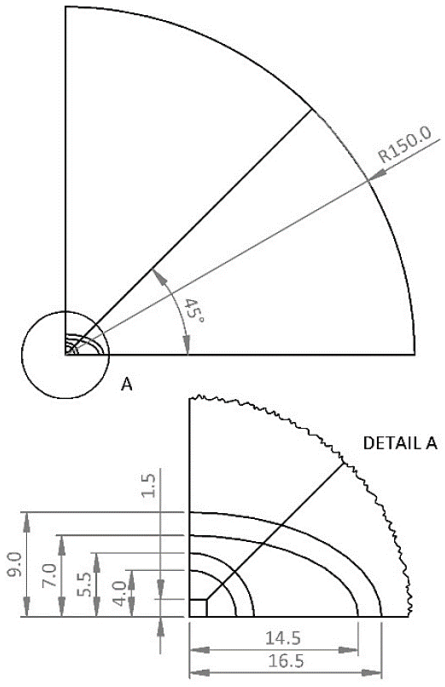

Fig. 3. The bottom view of the computational domain of the elliptical IDF burner (all dimensions are in mm).

2.2 Grid Construction

As previously stated, the domain's inlet side was partitioned into multiple geometries to simplify the grid generation process. This division enables the application of hexahedral mesh type, which is preferable for CFD simulations due to its accuracy and efficiency in resolving flow gradients compared to tetrahedral mesh. A variable cell size was employed in the model's region of interest corresponding to the flame shape, as shown in Fig. 4. This refinement process was based on the prior experimental results reported in [20]. To resolve the exceedingly high shear layers between the air jet and the entrained fuel, the grid was densified in the flame core by a cell size of 0.1 mm, which increased axially and radially with a maximum element dimension of 4 mm in both radial directions and 7.5 mm in the axial direction. The total number of cells amounted to 1,732,500 cells. Regarding the grid quality, the skewness minimum, maximum, and average values were 5e-8, 0.58, and 0.13, respectively, with a standard deviation of 0.12.

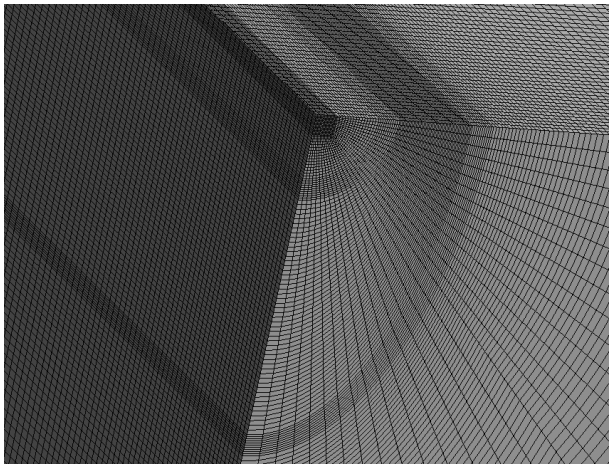

Fig. 4. A 3-D view of the generated computational grid.

2.3 Boundary Conditions

Both air and fuel are supplied at room temperature and atmospheric pressure. The air jet bulk velocity is kept at three values, i.e., 13.26, 15.58, and 17.90 m/s, while the fuel is kept constant at 0.026 m/s to match the experimental boundary conditions provided in [20]. Fig. 2 demonstrates the boundary conditions assigned to the computational model. The opening boundary condition is exposed to the atmospheric air, i.e., composition, temperature, and pressure. The pressure output is considered the atmospheric pressure.

2.4 Turbulence Model

The k-ε and BSL EARSM models are two of the commonly used turbulence models in CFD. They are both two-equation models, meaning they solve transport equations for the turbulent kinetic energy (k) and its dissipation rate (ε) or specific dissipation rate (ω). The k-ε model is based on the standard or realizable eddy viscosity assumption, while the BSL EARSM model is an explicit algebraic Reynolds stress model that accounts for the anisotropy of the Reynolds stresses. The BSL EARSM model is derived from a pressure-strain correlation model that incorporates compressibility effects and uses the weak-equilibrium assumption to obtain an explicit expression for the Reynolds stress tensor. The k- ε and BSL EARSM models have different strengths and weaknesses depending on the flow scenario. For example, the k- ε model tends to perform better for wall-bounded flows, while the BSL EARSM model can capture more accurately the effects of mean flow rotation, strain, and shear on the turbulence structure. So, a comparison of these models for inverse jet diffusion flames is provided in the current study.

2.5 Combustion Model

In this study, the Eddy dissipation model was employed, which enables the addition and definition of new reactions and materials without relying on predefined libraries. However, this model has a limitation in predicting radicals and intermediates (such as CO) accurately, as it assumes complete combustion to a large extent. Therefore, it tends to overestimate the adiabatic flame temperature and CO_2 emissions (and underestimate CO emissions) especially in regions with fuel-rich and near-stoichiometric conditions.

The following equation is used to calculate the mass fraction:

$$\frac{\partial Y_{\mathrm{i}}\rho}{\partial t}+\frac{\partial}{\partial x_{\mathrm{j}}}\left(\rho u_{\mathrm{j}}Y_{\mathrm{i}}\right)=\frac{\partial}{\partial x_{\mathrm{j}}}\left(\Gamma_{\mathrm{eff}}\frac{\partial Y_{\mathrm{i}}}{\partial x_{\mathrm{j}}}\right)+R_{\mathrm{f}} \tag{1}$$

The Eddy Dissipation model determines the reaction rate of fuel as follows:

$$R_{\mathrm{f}}=-A_{\mathrm{ebu}}\rho\frac{\varepsilon}{k}\min\left\{Y_{\mathrm{f}}\,,\quad\frac{Y_{\mathrm{o}}}{r_{\mathrm{f}}}\,,\quad B_{\mathrm{ebu}}\frac{Y_{\mathrm{p}}}{1+r_{\mathrm{f}}}\right\} \tag{2}$$

where: Y_f, Y_o and Y_p: mass fractions of fuel, oxidant, and product respectively, r_f = stoichiometry, and A_{ebu} and B_{ebu} are model constants.

2.6 Radiation Model

For spatial approximation, the discrete transfer model is adopted, while the spectral approximation is based on the gray model. The discrete transfer model offers high efficiency and is preferable in most cases, except when the solution involves directional sources or exhibits ray effects.

The discrete transfer model equations in CFX are based on the radiative transfer equation (RTE) that describes the change of radiant intensity along a ray path. The main assumption of the discrete transfer model is that the radiation leaving the surface element in a certain range of solid angles can be approximated by a single ray. The equation for the change of radiant intensity, I, along a path, s, can be written as:

$$\frac{dI}{ds}=-kI+kI_b \tag{3}$$

where k is the gas absorption coefficient and I_b is the blackbody intensity at the gas local temperature. The discrete transfer model integrates this equation along a series of rays emanating from boundary faces and calculates the net radiation heat flux on each surface and the energy source in the fluid due to radiation.

3. RESULTS AND DESCUSSION

3.1 Model Validation

In [20], the authors conducted experiments with LPG as the fuel, which actually contains up to seven different compounds. However, simulating the combustion of such a complex mixture would demand high computational resources. Therefore, this study investigates the effect of using a simplified LPG model, i.e., LPG (2), which consists of 70% Butane C_4H_{10} and 30% Propane C_3H_8 [19], versus using the full LPG composition, i.e., LPG (7) [21]. Moreover, the effect of two different turbulence models is also examined. This leads to conducting three numerical simulations in total, i.e., LPG (7)/BSL EARSM, LPG (2)/ BSL EARSM, and LPG (7)/k-ε.

Fig. 5 and Fig. 6 present the computational results of the three models along with the experimental data from [20] for the axial and radial flame temperature. As depicted in Fig. 5, the three models exhibit similar axial temperature profiles that agree well with the experimental data from Y = 150 mm above the burner rim to the downstream region of the flame. However, all models deviate from the experimental data in the near-burner region of the flame.

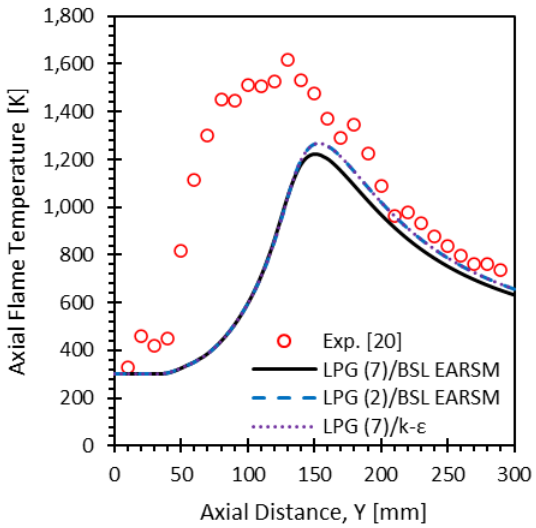

Fig. 5. The axial flame temperature distributions resulted from the three computational models.

Fig. 6 depicts the radial temperature profiles at two axial locations (Y = 30 and 120 mm). It reveals a reasonable agreement between the computational and experimental results, especially near the burner outlet. However, as the distance from the burner increases, some discrepancy emerges, although the shape of the radial distribution is maintained.

The axial and radial temperature profiles are very similar for LPG (7) and LPG (2) models, which suggests that simplifying the LPG to only two compounds can yield the same results as the full-LPG composition with lower computational expense. On the other hand, a comparison of the radial temperature profiles of the k-ε and BSL EARSM models shows that the k-ε model deviates more from the experimental data than the BSL EARSM model. This can be explained by the different formulations and assumptions of these two turbulence models. Both models are two-equation models, but the k-ε model assumes an eddy viscosity relation between the Reynolds stress tensor and the mean strain rate tensor, while the BSL EARSM model explicitly computes the Reynolds stress tensor from a pressure-strain correlation model. The BSL EARSM model accounts for the anisotropy of the Reynolds stresses and the effects of mean flow rotation, strain, and shear on the turbulence structure, which are important factors in inverse jet diffusion flames. Therefore, the BSL EARSM model can capture more accurately the radial temperature distribution of these flames than the k-ε model, as shown in Fig. 6.

So, LPG (2)/ BSL EARSM model is chosen to be used in the next simulations to assess the effect of air jet velocity.

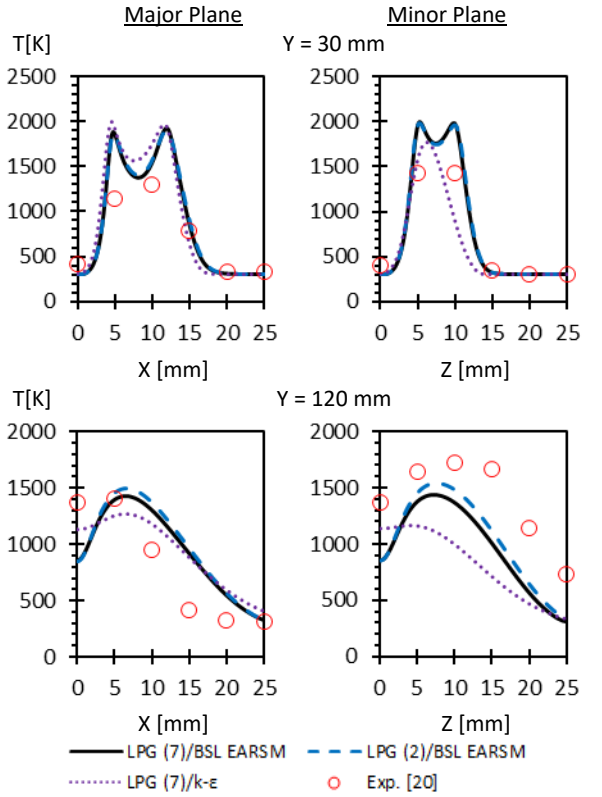

Fig. 6. The temperature radial profiles resulted from the three computational models.

3.2 Flame Temperature

Fig. 7 displays the temperature contours for the major and minor planes. Four distinct regions of the temperature distribution can be classified into: (1) the base flame region, (2) the merging region, (3) the inner reaction region, and (4) the post-combustion region. The temperatures in the base flame region are quite low because of the low-temperature fresh reactants. The base flame contains a cool core that is located in the air jet's potential core region. In the merging region, the chemical reactions cause the temperature of the flame to gradually rise from the neck of flame, while the temperature at the core of the flame remains cold owing to the existence of the air jet at the flame axis. The highest flame temperature is frequently linked with the inner reaction region. This is because of the air/fuel mixing procedure completion and the extra heat release. The post-combustion region is linked with the diminution in the temperature owing to the ambient air entrainment that cools down the hot combustion products, in addition to the reduced heat released. In the vicinity of the inner reaction cone, it can be noticed that the temperature contours are dense.

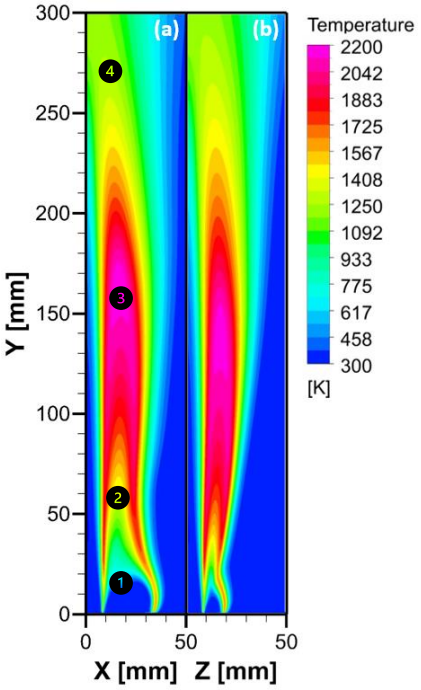

Fig. 7. Flame temperature contours for (a) major plane and (b) minor plane, at 15.58 m/s air jet velocity.

Fig. 8 shows the flame centerline temperatures as a function of the axial distance Y for three different air velocities and constant fuel velocity. The peak value generally implies that the centerline temperature decreases as the air velocity increases. This is because increasing the air velocity leads to cooling down the flame core even though the heat input is constant. For all flames, the mean centerline temperatures are nearly constant up to Y = 50 mm. Then, the temperature rises sharply to the inner reaction region. After that, it declines gradually as it moves through the post-combustion region. This is because the combustion products are diluted and cooled down by the entrained cold ambient air.

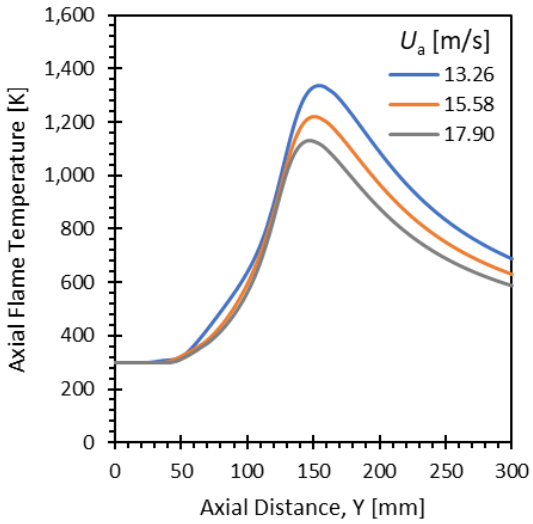

Fig. 8. Axial flame temperature distribution with varying air jet velocity at constant fuel velocity of 0.026 m/s.

Fig. 9 depicts the radial temperature profiles at the axial locations Y = 30 and 120 mm with varying the air jet velocity from 13.26 to 17.90 m/s at constant fuel velocity of 0.026 m/s. At Y = 30 mm (the merging region), all the flames exhibit similar temperature profiles with a slight increase in the temperature as the air velocity increases due to increasing the entrained fuel. On the contrary, at Y = 120 mm (post-flame region), the temperature profiles decrease as the air jet velocity increases due to entraining more ambient air.

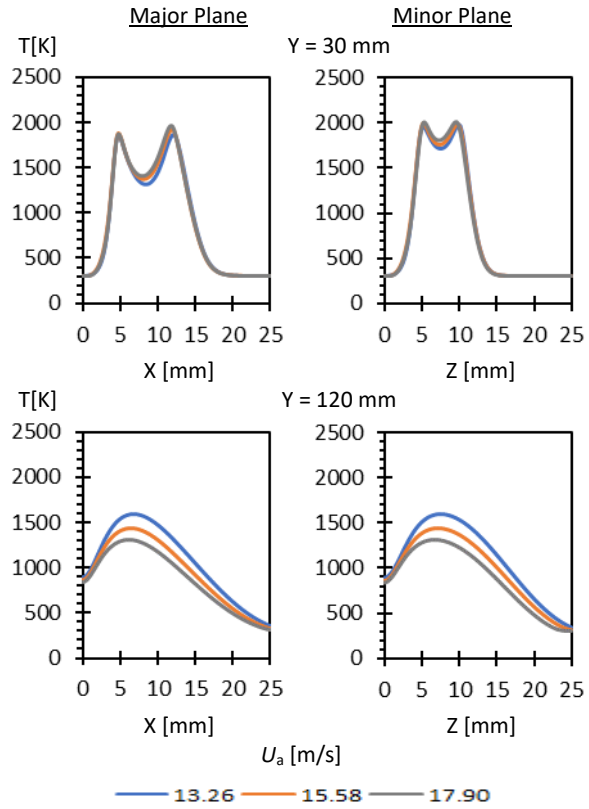

Fig. 9. Radial flame temperature distributions with varying air jet velocity at constant fuel velocity.

3.3 In-Flame Species

As depicted in Fig. 10, increasing the air jet velocity entrains more fuel to the flame core near the burner outlet, which leads to premixing more fuel in the air jet. This causes faster fuel consumption and lower LPG concentrations along the flame axis.

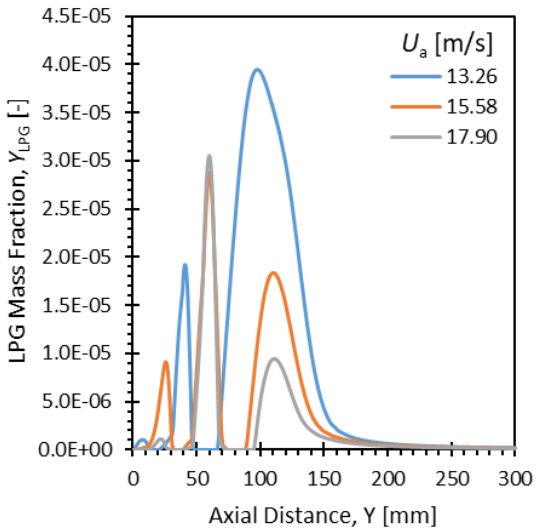

Fig. 10. Axial LPG mass fraction distributions with varying air jet velocity at constant fuel velocity.

Fig. 11 displays the radial profiles on both major and minor planes for the LPG mass concentrations.

Increasing the air jet velocity has a similar effect on the radial profiles, where the LPG concentrations decrease with higher air velocity due to the increased fuel entrainment toward the flame core, which premixes and consumes the LPG faster. Due to the elliptical shape of the fuel port, it can be noticed that for all flames, LPG has higher concentrations on the major plane than the minor plane.

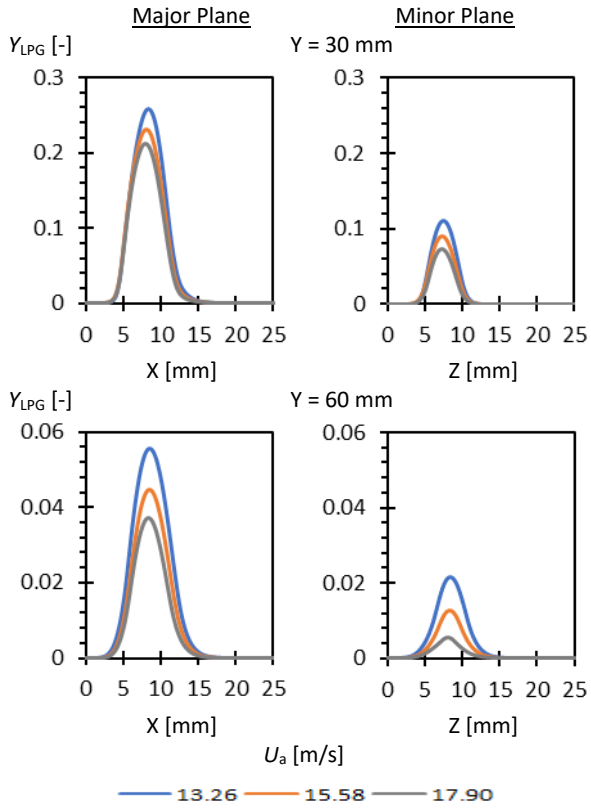

Fig. 11. Radial LPG mass fraction distributions with varying air jet velocity at constant fuel velocity.

Increasing the air jet velocity leads to decreasing the CO concentrations in both axial and radial directions. Fig. 12 depicts the axial distribution of the CO concentrations. The peak value occurs in the inner reaction zone and decreases with increasing the air jet velocity. This could be explained by shifting the flame toward the premixed mode with increasing the air jet velocity. This could be also observed in the radial profiles shown in Fig. 13.

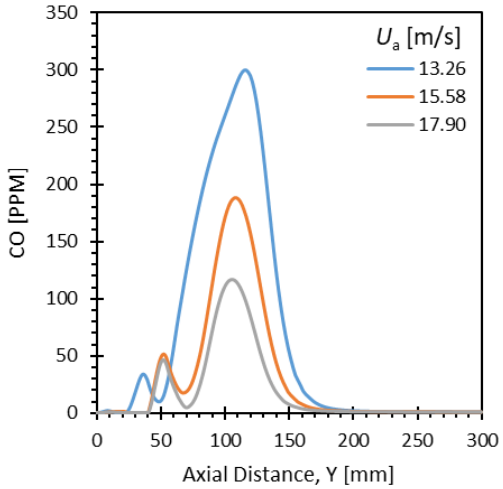

Fig. 12. Axial CO concentration distributions with varying air jet velocity at constant fuel velocity.

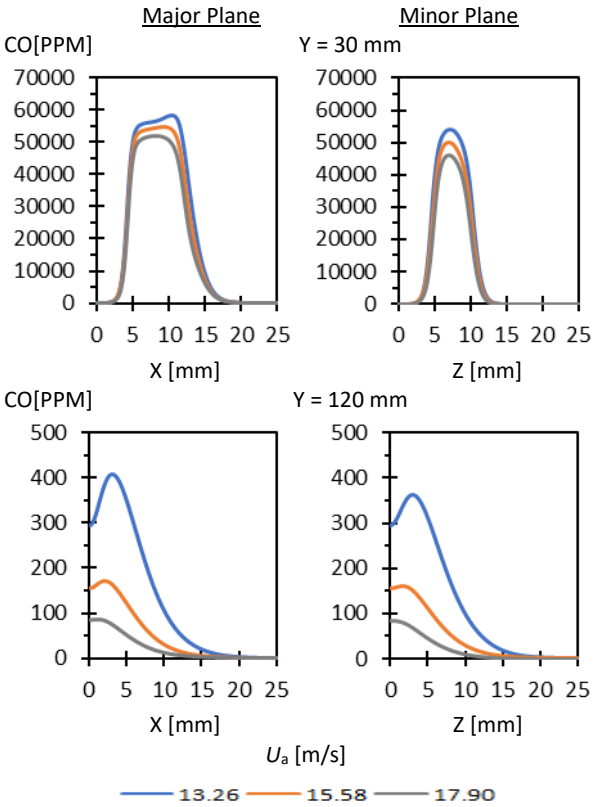

Fig. 13. Radial CO concentration distributions with varying air jet velocity at constant fuel velocity.

As mentioned before, increasing the air jet velocity leads to decreasing the flame temperature. Consequently, the thermal NO_X concentration decreases with increasing the air jet velocity, as depicted in Fig. 14. The figure also shows that the peak value appears inside the inner reaction region at Y > 150 mm above the burner outlet. This can be also noticed in the radial profiles (Fig. 15) at Y = 120 mm. However, in the near-burner region of the flame (Y = 30 mm), the radial profiles in the major plane show an opposite trend, where increasing the air velocity results in increasing the NO_X concentrations. This could be explained by the diffusion mode of the main flame, which creates a high-temperature reaction zone in the major plane. This region boosts thermal NO_X production when diluted with more air.

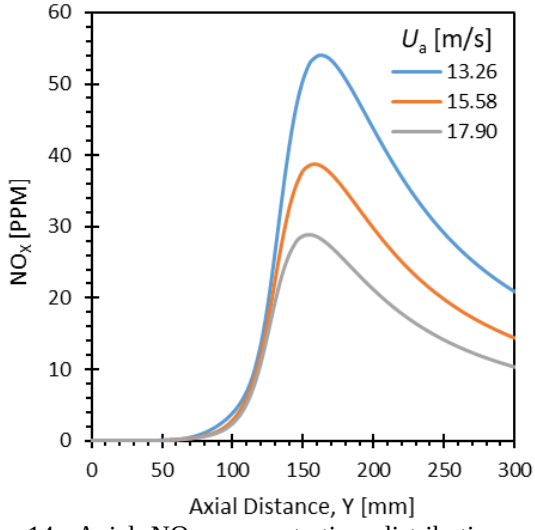

Fig. 14. Axial NO_X concentration distributions with varying air jet velocity at constant fuel velocity.

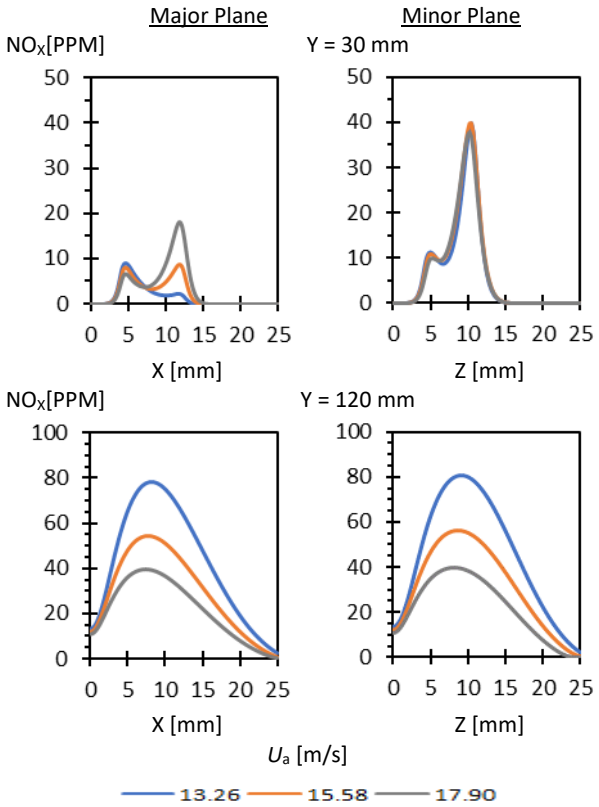

Fig. 15. Radial NO_X concentration distributions with varying air jet velocity at constant fuel velocity.

4. CONCLOSIONS

This study numerically investigated the effect of central air velocity on the flame and combustion characteristics of IDFs with elliptical jets at constant thermal input. The computational model was validated with previous experimental data and showed good agreement in terms of flame temperature. The study compared different turbulence, combustion, and radiation models and found that the BSL EARSM model and the simplified LPG model were suitable for simulating IDFs with elliptical jets.

The study revealed that increasing the air velocity resulted in lower flame temperature, LPG concentration, CO concentration, and NO_X concentration along the flame axis and radially. This was attributed to the enhanced fuel entrainment and mixing with the air jet, which shifted the flame toward the premixed mode and reduced the thermal NO_X production.

Based on the results reviewed, this burner configuration contributes to the understanding of IDFs characteristics and their potential applications in energy and thermal processes, such as heating, power generation, and propulsion.

5. REFERENCES

[1] Patel, V. and Shah, R., Effect of swirl and number of swirler vanes on combustion characteristics of methane inverse diffusion flame, Journal of Mechanical Science and Technology 33(4) (2019) 1947-1958.

[2] Patel, V. and Shah, R., Experimental investigation on flame appearance and emission characteristics of LPG inverse diffusion flame with swirl, Applied Thermal Engineering 137 (2018) 377-385.

[3] Hariharan, V. and Mishra, D.P., Static Flame Stability of Circumferentially Arranged Fuel Port Inverse Jet Non-Premixed Flame Burner, Combustion Science and Technology 192(8) (2019) 1493-1519.

[4] Sze, L.K., Cheung, C.S., and Leung, C.W., Appearance, temperature, and NOx emission of two inverse diffusion flames with different port design, Combustion and Flame 144(1-2) (2006) 237-248.

[5] Elbaz, A.M. and Roberts, W.L., Experimental study of the inverse diffusion flame using high repetition rate OH/acetone PLIF and PIV, Fuel 165 (2016) 447-461.

[6] Mikofski, M., Williams, T., Shaddix, C., and Blevins, L., Flame height measurement of laminar inverse diffusion flames, Combustion and Flame 146(1-2) (2006) 63-72.

[7] Mikofski, M.A., Williams, T.C., Shaddix, C.R., and Blevins, L.G., Effect of Varied Air Flow on Flame Structure of Laminar Inverse Diffusion Flames, in 2004 Spring Meeting, Western States Section /The Combustion Institute. 2004: United States.

[8] Sobiesiak, A. and Wenzell, J.C., Characteristics and structure of inverse flames of natural gas, Proceedings of the Combustion Institute 30(1) (2005) 743-749.

[9] Mahesh, S. and Mishra, D.P., Flame structure of LPG-air Inverse Diffusion Flame in a backstep burner, Fuel 89(8) (2010) 2145-2148.

[10] Elbaz, A.M. and Roberts, W.L., Experimental Characterization of Methane Inverse Diffusion Flame, Combustion Science and Technology 186(9) (2014) 1249-1272.

[11] Dong, L.L., Cheung, C.S., and Leung, C.W., Heat transfer characteristics of an impinging inverse diffusion flame jet – Part I: Free flame structure, International Journal of Heat and Mass Transfer 50(25-26) (2007) 5108-5123.

[12] Zhen, H.S., Leung, C.W., and Cheung, C.S., Thermal and emission characteristics of a turbulent swirling inverse diffusion flame, International Journal of Heat and Mass Transfer 53(5-6) (2010) 902-909.

[13] Zhen, H.S., Leung, C.W., and Cheung, C.S., A comparison of the thermal, emission and heat transfer characteristics of swirl-stabilized premixed and inverse diffusion flames, Energy Conversion and Management 52(2) (2011) 1263-1271.

[14] Stelzner, B., Hunger, F., Voss, S., Keller, J., Hasse, C., and Trimis, D., Experimental and numerical study of rich inverse diffusion flame structure, Proceedings of the Combustion Institute 34(1) (2013) 1045-1055.

[15] Shah, R., Experimental and Numerical Investigation of LPG-Fueled Inverse Diffusion Flame in a Coaxial Burner, International Journal of Advanced Thermofluid Research 3(1) (2017) 16-28.

[16] Khudhair, R. and Jung, Y. Environmental and Economical Evaluation of Liquified Natural Gas Vehicles Promotion Program in The City of Baghdad. in Proceedings of the 8th International Exchange and Innovation Conference on Engineering & Sciences (IEICES 2022). 2022. Kyushu University, Fukuoka, Japan (Hybrid).

[17] Abdelhameed, E. and Tashima, H. An investigation on the behavior of the torch flame in the LBGE combustion process. in Proceedings of the 8th International Exchange and Innovation Conference on Engineering & Sciences (IEICES 2022). 2022. Kyushu University, Fukuoka, Japan (Hybrid).
[18] Saleh, H., Effect of variation in LPG composition on emissions and performance in a dual fuel diesel engine, Fuel 87(13-14) (2008) 3031-3039.
[19] Elbaz, A.M., Moneib, H.A., Shebil, K.M., and Roberts, W.L., Low NOX - LPG staged combustion double swirl flames, Renewable Energy 138 (2019) 303-315.
[20] A. Mahgoub, A., M. Hussien, A., and A. Emara, K., Experimental Investigation of Stability and Structure of Vertical LPG Inverse Diffusion Flames Issuing from an Elliptic Burner, Engineering Research Journal 171(0) (2021) 119-137.
[21] S. Mohamed Gamal, M., M. Abdulnaim, A., A. Emara, A., and A. Moneib, H., CFD Modelling of CH4/Air Flames Characteristics Issuing from a Two-Slot EV-Burner, Engineering Research Journal 176(0) (2022) 171-184.